GEOPHYSICS. VOL. 77, NO. 1 (JANUARY-FEBRUARY 2012); P. E33–E42, 11 FIGS., 3 TABLES.
10.1190/GEO2010-0298.1

Bayesian inversion of CSEM and magnetotelluric data

Arild Buland[1] and Odd Kolbjørnsen[2]

ABSTRACT

We have developed a Bayesian methodology for inversion of controlled source electromagnetic (CSEM) data and magnetotelluric (MT) data. The inversion method provided optimal solutions and also the associated uncertainty for any sets of electric and magnetic components and frequencies from CSEM and MT data. The method is based on a 1D forward modeling method for the electromagnetic (EM) response for a plane-layered anisotropic earth model. The inversion method was also designed to invert common midpoint (CMP)-sorted data along a 2D earth profile assuming locally horizontal models in each CMP position. The inversion procedure simulates from the posterior distribution using a Markov chain Monte Carlo (McMC) approach based on the Metropolis-Hastings algorithm. The method that we use integrates available geologic prior knowledge with the information in the electromagnetic data such that the prior model stabilizes and constrains the inversion according to the described knowledge. The synthetic examples demonstrated that inclusion of more data generally improves the inversion results. Compared to inversion of the inline electric component only, inclusion of broadside and magnetic components and an extended set of frequency components moderately decreased the uncertainty of the inversion. The results were strongly dependent on the prior knowledge imposed by the prior distribution. The prior knowledge about the background resistivity model surrounding the target was highly important for a successful and reliable inversion result.

INTRODUCTION

Electromagnetic (EM) methods used in geophysics can be divided into passive source and active source techniques. Magnetotellurics (MT) is a passive source technique that uses the natural EM energy due to solar wind interacting with the earth's magnetic field as source. The MT data can give an image of large scale resistivity structures in the subsurface, but is, in practice, insensitive to thin resistive layers such as a hydrocarbon reservoir. The theory of MT was presented by Cagniard (1953). An application of MT onshore is presented by Vozoff (1972) and a more recent application of MT offshore is presented by Key et al. (2006).

The controlled source electromagnetic (CSEM) methods normally use electric dipole antennas as sources, in which the source strength is determined by the dipole length and electric current amplitudes. The first use of the marine CSEM method for direct detection of hydrocarbons is presented by Eidesmo et al. (2002), in which the method is introduced as seabed logging (SBL), and Ellingsrud et al. (2002) presents the first full-scale field test of SBL offshore Angola in 2000. In the following, we will concentrate on marine CSEM methods in which a horizontally electric dipole (HED) source is towed close to the seafloor and the EM receivers are positioned on the seafloor. If the recording of the EM data is continued for a sufficiently long time, typically some days, the data contain both the response from the active source (the CSEM data) and the MT data. The CSEM data contain a set of frequency components depending on the source signal and a set of different source-receiver offsets, whereas the marine MT data typically have a broader and lower frequency spectrum. In CSEM analysis, the MT data are considered as noise, but here, we will quantify the possible benefit of integrating the MT signals in the analysis.

Key (2009) presents a 1D isotropic Occam-type inversion aiming for a smooth model. Based on simple 1D models, he studies the resolution of joint inversion of various sets of frequencies and electric and magnetic components. Mackie et al. (2007) and Commer and Newman (2009) present joint 3D inversion of marine CSEM and MT data and demonstrate by a synthetic example that joint inversion better resolves the resistivity variations. In this paper, we will invert CSEM and MT data and quantify the uncertainty of the model parameters for different sets of frequencies and EM components.

Manuscript received by the Editor 12 September 2010; revised manuscript received 14 March 2011; published online 3 February 2012.
[1]Statoil, Stavanger, Norway; and University of Stavanger, Norway. E-mail: abu@statoil.com
[2]Norwegian Computing Center, Oslo, Norway. E-mail: odd.kolbjornsen@nr.no

It is well known that inversion of EM data is ill-posed, but the vast majority of published inversion methods and studies present a solution without any assessment of the uncertainty. From a statistical perspective, the solution of an inverse problem is not limited to one predicted model, but is represented by a probability density function (PDF) on the model space. The aim of inversion is not only to find a best-fitting set of model parameters but also to characterize the uncertainty in the inversion results. A Bayesian setting is a natural choice for many geophysical inverse problems. For an introduction, see, for example, Tarantola and Valette (1982); Tarantola (1987); Duijndam (1988a, b); Malinverno (2000); Scales and Tenorio (2001); Ulrych et al. (2001). Bayesian inversion is applied in several topics in geophysics, for example, amplitude variation with offset (AVO) inversion (Buland and Omre, 2003a, c; Buland et al., 2003; Gunning and Glinsky, 2004), wavelet estimation (Buland and Omre, 2003b; Gunning and Glinsky, 2006), lithology and fluid prediction (Larsen et al., 2006; Buland et al., 2008; Bosch et al., 2010; Kjønsberg et al., 2010; Rimstad and Omre, 2010; Grana and Rossa, 2010), and time-lapse analysis (Buland and El Ouair, 2006; Veire et al., 2006). In a Bayesian setting, available prior knowledge is combined with the information contained in the measured data. The prior knowledge about the model parameters is specified by PDFs in which the prior information and the corresponding uncertainty is defined. The relationship between the model parameters and the measured data is described by the likelihood model. The solution of a Bayesian inverse problem is represented by the posterior distribution, which provides both the most probable solution and information about the corresponding uncertainty. The uncertainty is needed both for correct interpretation and to correctly weight this information in integration with other knowledge and data.

Christensen and Dodds (2007) present an empirical noise model for the CSEM data and solved the 1D CSEM inversion problem by an iterative damped least-squares approach. They used a linearized approach to estimate the uncertainty of the model parameters based on analysis of the posterior covariance matrix. The linear approach assumes that the model response is local linear at and close to an estimated solution, and neglects any nonlinear effects. Key (2009) studies uncertainty of 1D CSEM inversion by inverting multiple data sets produced from one single synthetic model that added different realizations of noise. This approach shows the sensitivity of the solution to changes of the data, but does not include the uncertainty related to nonuniqueness, i.e., one single data set may have different solutions. Hoversten et al. (2006) and Hou et al. (2006) present deterministic and a minimum entropy method for saturation estimation by joint inversion of CSEM and seismic AVA data. Chen et al. (2007) present a Bayesian approach to the same joint inversion problem as in the two previous papers. Their results show that the uncertainty of the estimated saturation is reduced by joint CSEM and seismic AVA inversion compared to inversion of the seismic data alone. Gunning et al. (2010) discuss resolution and uncertainty aspects of isotropic 1D CSEM inversion based on approximate Bayesian approaches and conclude that linearization approaches to uncertainty analysis based on covariance matrices are of very limited use and underestimate the true uncertainty.

The next sections present Bayesian 1D EM inversion methodology using a complete and valid stochastic simulation method, results of inversion of synthetic data sets and then line inversion of CMP-sorted real data from the Troll field.

BAYESIAN EM INVERSION METHODOLOGY

We assume a layered earth model, where each layer is described by the thickness Δt and the horizontal resistivity R_h and the vertical resistivity R_v. The electrical anisotropy is often significant and can be represented by the anisotropy factor here defined as the ratio between vertical and horizontal resistivity $\gamma = R_v/R_h$. The top layer is always air that extends infinitely above the model, and the deepest layer extends down to infinity. To get a compact notation, all model parameters are collected in the model vector $\mathbf{m}$. The corresponding modeled EM response is denoted $\mathbf{f}(\mathbf{m})$, where $\mathbf{f}$ is a nonlinear vector function. The observed EM data are stored in the data vector $\mathbf{d}$, where the elements correspond directly to the elements in the modeled response vector $\mathbf{f}(\mathbf{m})$. The aim of the inversion is to estimate the model parameters in $\mathbf{m}$, including the associated uncertainties and the dependencies between the different model parameters. In Bayesian inversion, the complete solution is represented by the posterior distribution. This will be explained in the following.

EM forward modeling

The EM response $\mathbf{f}(\mathbf{m})$ is defined by Maxwell's equations. In general, both the model parameters and the electric and magnetic fields vary in a 3D space, but a practical problem is that forward modeling of 2D and 3D models are highly computer-demanding tasks. A practical solution for simple geological settings is to calculate the 3D EM fields for 1D models varying only with depth. The response of a dipole embedded in a layered 1D earth model is described by several authors, e.g., Chave and Cox (1982). We use a forward modeling method for 1D anisotropic models described by Løseth and Ursin (2007).

The 1D approach is strictly valid only for plane-layered models with properties varying only in the depth direction. For simple geological settings, we extend the use of 1D modeling to model a survey line by assuming locally 1D models at certain locations along the line. We assume that this approach is an adequate approximation if the earth properties vary slowly laterally compared to the source-receiver offsets considered. Before inversion along a survey line, we sort and group the observed data into gathers with common source-receiver midpoint (CMP) positions. This is a standard sorting technique for seismic data, but also used for EM data; see, e.g., Mittet et al. (2007). Local 1D earth models are defined at each CMP location.

Bayes rule

Bayes rule defines the modified or posterior probability function as

$$p(\mathbf{m}|\mathbf{d}) \propto p(\mathbf{d}|\mathbf{m})p(\mathbf{m}), \tag{1}$$

where $\mathbf{d}$ is a vector of data, $\mathbf{m}$ is a vector of parameters defining the earth model, $p(\mathbf{d}|\mathbf{m})$ is the likelihood function and $p(\mathbf{m})$ is the prior distribution. To simplify the notation, we use a generic notation $p(\cdot)$ for a PDF in which the actual function is determined by the argument. The prior model $p(\mathbf{m})$ represents our knowledge and uncertainty about the model before we have the new data or information. A prior model is, in general, defined from all current geological knowledge about the subsurface rock properties. The likelihood model $p(\mathbf{d}|\mathbf{m})$ is defined by the forward modeling $\mathbf{f}(\mathbf{m})$ and an error model for the data $\mathbf{d}$. A model $\mathbf{m}$ with a small misfit between the modeled response $\mathbf{f}(\mathbf{m})$ and the real data $\mathbf{d}$ has a higher likelihood than a model with a large

misfit. The posterior distribution represents the complete solution of the Bayesian inversion, and provides an updated probability model with reduced uncertainties. The prior, likelihood and the posterior models are presented in the following.

The prior model

The prior probability distribution $p(\mathbf{m})$ represents our prior knowledge and uncertainty about the model before we start the inversion. In general, this is a multidimensional probability distribution including both the probability distributions for all the model parameters contained in $\mathbf{m}$ and also all dependencies between the model parameters.

We define the layers as stochastically independent in the prior model. This model allows us to study the resolution and nonuniqueness problems of separating a high-resistive target layer from other possible resistive layers above and below the target. A common alternative to a model with independent layers is to include correlation between the layers forcing the inversion to search for smooth solutions. A thin hydrocarbon reservoir with a thickness about 100 m may then typically be imaged as a smooth curve with a total thickness on the order of 1 km, and the peak resistivity will be far below the true reservoir resistivity. We will later see that this is similar to the results we get when we use a wide prior model allowing for high resistivity in the nontarget layers.

The resistivity of the subsurface can vary several orders of magnitude, e.g., 0.3 Ωm in seawater, typically in the order of 1–10 Ωm in brine-filled sandstones and shales, and up to 100 Ωm or more in hydrocarbon-filled reservoirs. Other lithologies, as for example, salt and nonporous rocks, may act almost as insulators with extremely high resistivity. To use simple standard distributions, for example, the uniform distribution, we find it practical to define the prior model for the logarithm of the resistivity instead of the resistivity directly.

The EM data usually have poor resolution compared with seismic data, and the definition of the structures of the model can, in practice, be done by seismic interpretation. If the quality of the seismic horizons is good, the EM data may not provide significant modifications of these, and an adequate approach may be to fix the layer boundaries defined by the seismic horizons. In our approach, the thickness Δt of a layer may have a certain probability of being zero such that the layer disappears. This can be modeled by a mixture of a discrete probability for zero thickness and a continuous distribution for the range of possible thicknesses. Another simple practical way of modeling this is to use a continuous distribution allowing for negative values, where negative thickness is interpreted as zero thickness.

The likelihood model

The likelihood model $p(\mathbf{d}|\mathbf{m})$ is defined by the forward modeling $\mathbf{f}(\mathbf{m})$ and an error model. Because the response of the EM data may vary over several magnitudes in strength it is important that the magnitude of the error is adjusted accordingly. We use a Gaussian error model that is on a scale proportional to the modeled response $\mathbf{f}(\mathbf{m})$. The likelihood model is a conditional Gaussian distribution for $\mathbf{d}$ for a given model $\mathbf{m}$,

$$p(\mathbf{d}|\mathbf{m}) = \frac{1}{(2\pi)^{n/2}|\Sigma(\mathbf{m})|^{1/2}} \times \exp\left\{-\frac{1}{2}[\mathbf{d}-\mathbf{f}(\mathbf{m})]^T[\Sigma(\mathbf{m})]^{-1}[\mathbf{d}-\mathbf{f}(\mathbf{m})]\right\}, \quad (2)$$

with expectation defined by the modeled response $\mathbf{f}(\mathbf{m})$ and covariance matrix $\boldsymbol{\Sigma}(\mathbf{m})$ depending on $\mathbf{f}(\mathbf{m})$. The dimension n is equal to the number of data samples in $\mathbf{d}$ and $\mathbf{f}(\mathbf{m})$. In general, a model $\mathbf{m}$ with a modeled response $\mathbf{f}(\mathbf{m})$ with a close match to the data $\mathbf{d}$ has a high likelihood, and vice versa.

Electromagnetic inversion is often defined for magnitude and phase data, but we define the likelihood model for complex data samples d_k, where index k runs over different frequencies, offsets, and EM components. We will here assume that the error for the real and the imaginary components are independent and have the same variances, defined as

$$\sigma^2(f_k(\mathbf{m})) = \sigma_R^2|f_k(\mathbf{m})|^2 + \sigma_{NF}^2, \quad (3)$$

where σ_R^2 and σ_{NF}^2 are the relative variance and noise floor variance, respectively. The contribution from the relative term is scaled with the magnitude of the modeled response, and then represents an error which is on the same scale as the modeled response for this sample. The contribution from the noise floor ensures that the error is not too small compared to the measuring device used to collect the data.

We model the error of the different data samples as independent giving a diagonal covariance matrix $\boldsymbol{\Sigma}$. The effect of possible correlated error is compensated by using a slightly larger standard deviation for the independent noise. The inversion method does not require a Gaussian likelihood model, but we regard this is as an adequate and sufficiently flexible model for the noise.

The posterior model

The complete solution of Bayesian inversion is represented by the posterior distribution $p(\mathbf{m}|\mathbf{d})$. From the posterior distribution, we can derive expectation values, standard deviations, correlation coefficients, and other statistical parameters of interest. In simple inversion settings, such as linear problems with Gaussian assumptions, it is possible to derive analytical expressions for the posterior distribution. For most inversion problems, however, we have to rely on stochastic simulation techniques. If we can simulate samples from the unknown posterior distribution, the solution of the inversion problem is represented by the simulated samples and we can easily calculate statistical properties such as expectation and variance.

Markov chain Monte Carlo (McMC) simulation is a general stochastic simulation technique with wide applicability in modern applied statistics. The idea of McMC is to generate random samples from a specific probability distribution by simulating a cleverly constructed Markov chain; see, e.g., Gilks et al. (1996) and Robert and Casella (1999). This is done by constructing a Markov chain with stationary distribution equal to the desired sampling distribution, which is the posterior distribution in Bayesian inversion. When the Markov chain has converged to its stationary distribution, each new state of the Markov chain is then also a sample from the desired sampling distribution. The Metropolis-Hastings algorithm, which was proposed by Metropolis et al. (1953) and later generalized by Hastings (1970), gives a very general recipe for construction of Markov chains with the required properties. Let $\mathbf{m}_c$ denote the current state of the Markov chain when we start iteration j, and let $\mathbf{m}_p$ be a new proposed state. The first step in a new iteration of the Metropolis-Hastings algorithm is to propose a model $\mathbf{m}_p$ by drawing from a specified proposal probability distribution $q(\mathbf{m}_p|\mathbf{m}_c)$. The next step is to calculate the acceptance probability P_a given by

$$P_a(\mathbf{m}_p, \mathbf{m}_c) = \min\left\{1, \frac{p(\mathbf{d}|\mathbf{m}_p)p(\mathbf{m}_p)q(\mathbf{m}_c|\mathbf{m}_p)}{p(\mathbf{d}|\mathbf{m}_c)p(\mathbf{m}_c)q(\mathbf{m}_p|\mathbf{m}_c)}\right\}. \quad (4)$$

The minimum function ensures that a proposed model will be accepted as the new current model with probability one if the product of the likelihood, prior, and proposal PDF in the nominator is larger than for the current model in the denominator. A proposed model with a lower product than the current model will be accepted with a probability given by the ratio of the products. The iteration is completed by accepting the proposed model $\mathbf{m}_p$ as the new model from iteration j with probability P_a. If the proposed model is not accepted, the model sample from this iteration is set equal to the model sample from the previous iteration.

The pseudocode of the general Metropolis-Hastings algorithm is very simple:

- Iterate $j = 1, 2, \ldots$
  - propose a new model $\mathbf{m}_p(j)$ by drawing from $q(\mathbf{m}_p|\mathbf{m}_c)$
  - compute the acceptance probability P_a (see equation 4)
  - set $\mathbf{m}_c(j) = \mathbf{m}_p(j)$ with probability P_a, otherwise $\mathbf{m}_c(j) = \mathbf{m}_c(j-1)$

An important practical aspect of McMC simulation is the choice of the proposal function. In our case, we use two simple proposal mechanisms that are the independence sampler and a random walk Metropolis-Hastings. The independence sampler is constructed such that it always proposes a completely new state from the prior distribution (independent of the current state)

$$q(\mathbf{m}_p|\mathbf{m}_c) = p(\mathbf{m}). \quad (5)$$

In this case, the acceptance probability simplifies to the likelihood ratio

$$P_a(\mathbf{m}_p, \mathbf{m}_c) = \min\left\{1, \frac{p(\mathbf{d}|\mathbf{m}_p)}{p(\mathbf{d}|\mathbf{m}_c)}\right\}. \quad (6)$$

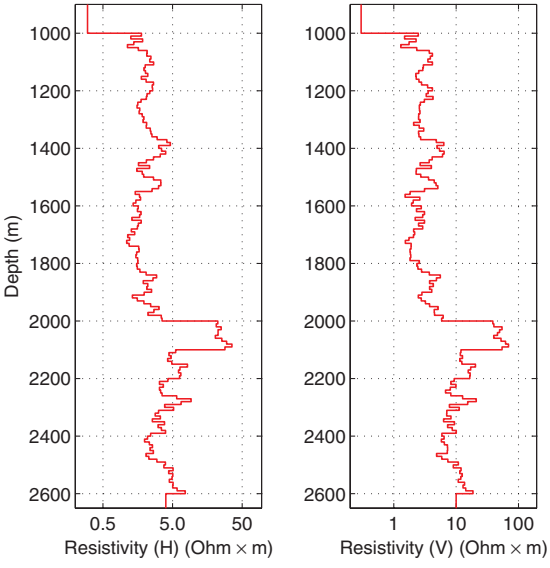

Figure 1. Reference case. Resistivity profile of the earth, left display is the horizontal resistivity, right display shows the vertical resistivity.

This means that a proposed new state is always accepted if the likelihood for the proposed model is higher than for the current model. However, the independence sampler will typically propose a lot of unlikely models with poor match between the modeled and the real data. A proposed model with lower likelihood than the current model may still be accepted if the likelihood is not too bad, but the acceptance probability will typically approach zero for a large set of models proposed from the prior model.

The random walk algorithm proposes a new state that is an adjustment of the current state. A simple example of a random walk proposal distribution is a uniform distribution centered in the current state:

$$q(\mathbf{m}_p|\mathbf{m}_c) = U(\mathbf{m}_c - s\Delta\mathbf{m}; \mathbf{m}_c + s\Delta\mathbf{m}), \quad (7)$$

where $\Delta\mathbf{m}$ is the range of the parameter $\mathbf{m}$, and s is a scalar scaling less than one. In this case, the acceptance probability simplifies to the posterior ratio

$$P_a(\mathbf{m}_p, \mathbf{m}_c) = \min\left\{1, \frac{p(\mathbf{d}|\mathbf{m}_p)p(\mathbf{m}_p)}{p(\mathbf{d}|\mathbf{m}_c)p(\mathbf{m}_c)}\right\}. \quad (8)$$

The uniform proposal mechanism in the random walk algorithm above may generate models that are outside the definition set for the earth parameters. A simple way to handle this problem is to set the acceptance probability to zero for all illegal models (models with zero prior probability). There is then no need to do any further edge correction in the acceptance probability because we have no edge correction in the proposal distribution. If the scaling number s in expression 7 is large, the random walk algorithm will have the same weakness as the independence sampler, by proposing many models that are not accepted. If the scaling number is small, the algorithm will propose models in the neighborhood of previously accepted models, which result in a high acceptance ratio. A potential problem with random walk simulation with small update steps is that the simulation may be trapped in the neighborhood of one out of several modes. In statistical simulation, this is often referred to as mixing, while in optimization theory the related problem is to be trapped in local minimums. To avoid these problems, we use multiple scalings. Typical selections of the scaling number s in equation 7 is: 0.005, 0.01, 0.02, 0.05, 0.1, and 0.2. In practical situations, one should always run multiple chains to check if the results converge and mix well.

SYNTHETIC INVERSION EXAMPLES

In this section, we present a synthetic inversion example using the Bayesian approach. We illustrate the uncertainty of the inversion results and investigate the impact of different field components and frequencies. We also show how prior knowledge about the subsurface resistivity constrains the inversion results and the importance of integrating the EM analysis with other known information.

Inversion setup

We have defined a 1D reference model with layers of 10-m thickness, see Figure 1. The model has a 100-m-thick high-resistivity layer buried 1000 m below the seafloor with horizontal resistivity approximately 25 Ωm. The horizontal resistivity fluctuates around 2 Ωm in the layers above the target and about 4 Ωm in the layers

below. The anisotropy factor fluctuates around 1.5, 2.0, and 2.5 in the layers above, in, and below the target, respectively. The seawater has a resistivity of 0.3 Ωm and the seafloor is at 1000-m depth.

We model electric and magnetic components for different source-receiver offsets along a line in the x-direction. The source dipole antenna is oriented both along the line (inline configuration) and perpendicular to the line (broadside configuration). In this study we consider three different sets of components:

1) inline electric component (E_x)
2) inline and broadside electric components (E_x, E_y)
3) inline and broadside electric and magnetic components (E_x, E_y, H_x, H_y)

The CSEM data are collected for two different frequency designs:

1) standard frequency set (S): 0.25 Hz, 0.75 Hz, and 1.25 Hz
2) extended frequency set (E): 0.1 Hz, 0.2 Hz, 0.4 Hz, 0.8 Hz, 1.6 Hz, 3.2 Hz, 6.4 Hz, and 12.8 Hz

For frequencies less than or equal to 0.25 Hz, the max offset is 9000 m; for frequencies between 0.4 Hz and 1.6 Hz, the max offset is 6000 m; and for higher frequencies, the max offset is 3000 m. For all frequencies, the offset spacing and the minimum offset is 300 m.

We do not add noise to the modeled reference data, but we define a realistic error model. The error model defines the likelihood model and determines the likelihood of a specific model depending on how the synthetic model response matches within the error model of the data. For example, if we assume noisy data with large data errors, a wide span of models will be accepted as likely if the modeled response is within the error model of the data. In the following test example, the noise floor varies with components and frequencies. For the electric components, it is 5×10^{-14} for the frequencies 0.4 Hz and below, and 1×10^{-14} for frequency 0.75 Hz and above. The noise floor for the magnetic component is 1000 times that of the electric components. The relative error is modeled to be 15%, which is larger than one normally would expect to account for the lack of coloration of the error. The passive MT data are modeled for 21 periods ranging from 10 to 1000 s, at an uniform spacing on the logarithmic scale, and is assumed to have a relative error of 10%.

We use a stochastic inversion model below the sea floor, and keep the air and water parameters fixed in this example. The model used for the inversion is coarser than the detailed reference model, and consists of 10 layers above the reservoir and five layers below the reservoir in addition to a half-space. We define two different prior models for the background layers:

1) a focused prior (F) in which the nonreservoir layers have a narrow span
2) a wide prior (W) in which the nonreservoir layers have a larger span

The prior distributions for the thickness, logarithm of the resistivity, and the anisotropy may be any legal probability distributions representing our prior knowledge. In this test, we have used uniform distributions with ranges as given in Table 1.

We run a total of 16 different inversion tests with different prior models and different subsets of the data, see Table 2. For each inversion, we run four parallel chains with one millon iterations and use these data to investigate the posterior. This is to check and ensure convergence. The speed is about 12,000 iterations per hour.

Inversion results

The three last columns in Table 2 summarize the inversion results by a measure of data fit, and the mean and spread of the vertical resistivity in the target layer. The data fit is given by chi-squared statistics, see Key (2009), which is the average deviation between modeled response and data relative to prior standard deviation:

$$\text{Fit} = \sqrt{\frac{1}{N \cdot n} \sum_{l=1}^{N} \sum_{k=1}^{n} \frac{(d_k - f_k(\mathbf{m}_l))^2}{\sigma^2(f_k(\mathbf{m}_l))}}, \tag{9}$$

where N is the number of simulated models and n is the number of data samples. If the error model defined by the variance σ^2 in the denominator matches the size of the misfit in the nominator, this quantity should be about one. In our case, it will generally be lower than one because we have not added noise to the reference data. All runs have a good average data fit substantially below one.

The interquartile range is a measure of the spread of a distribution, and is defined as the length of the interval that contains the central 50% of the realizations, i.e., the distance from the P25 to the P75 percentile. We compute this length in the logarithmic domain and report the normalized interquartile range (nIQR), which is the ratio of the posterior to the prior interquartile range. If there is no information in the data, the uncertainty will not be reduced by the inversion and nIQR will be close to one. The nIQR represents the uncertainty after inversion relative to the prior uncertainty.

The first row in Table 2 (run 0) shows the results of a simulation from the prior model. The prior model for the resistivity in the target layer is defined by a uniform distribution from 1 to 100 Ωm for the logarithm of the horizontal resistivity, and a uniform distribution from 1 to 3 for the anisotropy factor R_v/R_h. This gives a prior mean vertical resistivity in the target layer of about 42.5 Ωm. Because no data are inverted in this case, the uncertainty equals the prior uncertainty, and nIQR is, per definition, equal to one.

In runs 1–3, we use a focused prior model illustrating a case with relatively good knowledge about the subsurface resistivities both

Table 1. Summary of the focused and wide prior models for inversion. The table shows ranges for layer thickness, horizontal resistivity, and anisotropy for the two models. Number of layers are in parentheses.

Model	Layer (no.)	Thickness (m)	Resistivity (Ωm)	Anistropy
Both	Air (1)	∞	10^{13}	1.0
	Water (1)	1000	0.3	1
Focused	Above (10)	90–110	1–3	1–2
	Target (1)	50–200	1–100	1–3
	Below (5)	90–110	2–6	2–3
	Half-space (1)	∞	2–6	2–3
Wide	Above (10)	90–110	1–5	1–4
	Target (1)	50–200	1–100	1–3
	Below (5)	90–110	2–10	2–4
	Half-space (1)	∞	2–10	2–4

Table 2. Inversion setup and summary of the inversion results with reference numbers in column 1. Run 0 refers to the prior model. Column 2 defines focused (F) or wide (W) prior models, column 3 defines the subset of the EM components used in the inversion, column 4 defines standard (S) or extended (E) frequency set, and column 5 shows whether MT-data was included (+) or not (−). Columns 6–8 summarize inversion statistics: The inversion fit, mean resistivity in target layer, and the normalized interquartile range (nIQR) in the target layer.

Run	Prior	EM	Freq.	MT	Fit	Mean (Ωm)	nIQR
0						42.5	1.00
1	F	-	-	+	0.24	54.6	0.84
2	F	1	S	-	0.19	58.8	0.22
3	F	3	E	+	0.10	51.9	0.17
4	W	-	-	+	0.21	41.7	0.99
5	W	1	S	-	0.23	23.0	0.58
6	W	1	E	-	0.20	22.0	0.54
7	W	1	S	+	0.21	17.5	0.48
8	W	1	E	+	0.19	19.5	0.50
9	W	2	S	-	0.18	14.5	0.50
10	W	2	E	-	0.14	23.4	0.41
11	W	2	S	+	0.17	15.4	0.48
12	W	2	E	+	0.14	23.5	0.42
13	W	3	S	-	0.14	17.4	0.47
14	W	3	E	-	0.11	28.2	0.29
15	W	3	S	+	0.14	16.9	0.49
16	W	3	E	+	0.11	24.7	0.34

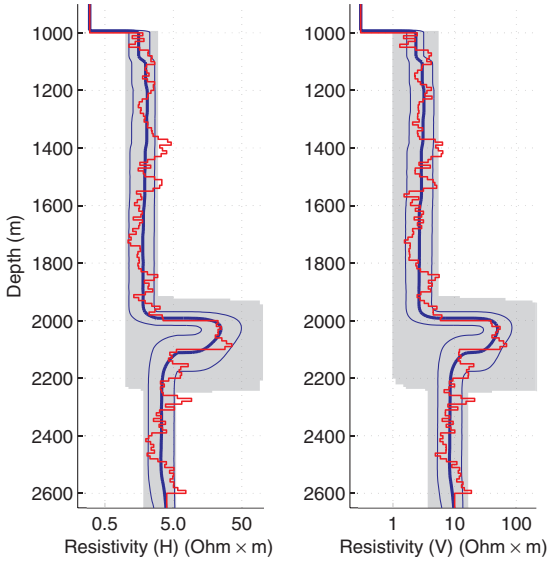

Figure 2. Inversion results for focused prior, CSEM inline electric component E_x and standard frequency set. The left panel shows the horizontal resistivity, and the vertical resistivity is on the right. The thick blue curve is the median at each depth point, the thin blue curves are the P10 and the P90 quantiles. The original curve is in red, and the shaded gray area shows the prior range.

above and below the target layer. In runs 4–16, we use a wide prior model representing a situation with weak prior knowledge. These cases illustrate the severe resolution problems in EM inversion and the need for additional prior knowledge to constrain the inversion. The prior model for the target layer is the same for all tests; see all details in Table 1.

The inversion result for a focused prior model and a standard CSEM survey with electric inline component and standard frequency set (run 2) is illustrated in Figure 2, showing P10, P50 (median), and P90 for the resistivities as a function of depth. The anomaly is well localized by the median of both the horizontal and the vertical resistivity. The inverted horizontal resistivity has only a weak sensitivity for a thin resistor (Løseth and Ursin, 2007), and usually will not be detected by unconstrained inversion. In this example, the inversion finds the high horizontal resistivity with the help of the prior model restricting the anisotropy factor between one and three in the target layer.

The marginal distributions at each depth displayed in Figure 2 hide the correlation structures between different layers. Figure 3 shows four different accepted resistivity profiles. Note in particular, the thickness versus resistivity tradeoff in the target layer, i.e., thick layers have low resistivity and thin layers have high resistivity. This is in agreement with the results in Constable and Weiss (2006) in which the thickness versus resistivity problem is discussed. Figure 4 displays the modeled EM response corresponding to the different resistivity profiles in Figure 3, in which all show a good match to the data.

In run 2, the mean vertical resistivity in the target layer is estimated to 58.8 Ωm , and the uncertainty measured by the normalized interquartile range (nIQR) is reduced to 22% of the prior uncertainty. When the extended frequency set (E) is used in run 3, the mean vertical resistivity in the target layer is estimated to 51.9 Ωm, and the uncertainty (nIQR) is reduced to 17% of the prior uncertainty. Inversion of only MT-data in run 1 reduces the uncertainty (nIQR) only to 84% of the prior uncertainty.

In runs 4–16, we use a wide prior model for the nontarget layers to illustrate the problems when the prior knowledge is vague. Run 5 has the same setup as run 2 using the inline electric component and the standard frequency set. Comparison of the results for these two runs shows the effect of changing the prior distribution. Figure 5 displays the results for run 5. The anomaly in the target layer is less pronounced in this inversion than it was for the focused prior, the uncertainty above and below the target is also larger. In the target layer, the mean vertical resistivity is estimated to only 23 Ωm, and the uncertainty (nIQR) is reduced only to 58% of the prior uncertainty. The reason for the low mean target resistivity is that the nontarget layers are now allowed to have high resistivity; see Table 1.

The effect of including more data in the setting with a vague prior model can be investigated by comparing run 5 with run 16 in which the maximum amount of data is used, i.e., MT data and CSEM

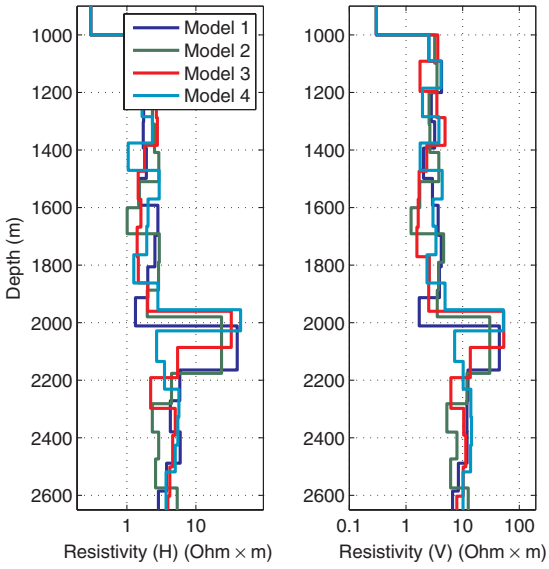

Figure 3. Four resistivity profiles from the posterior distribution in run 2.

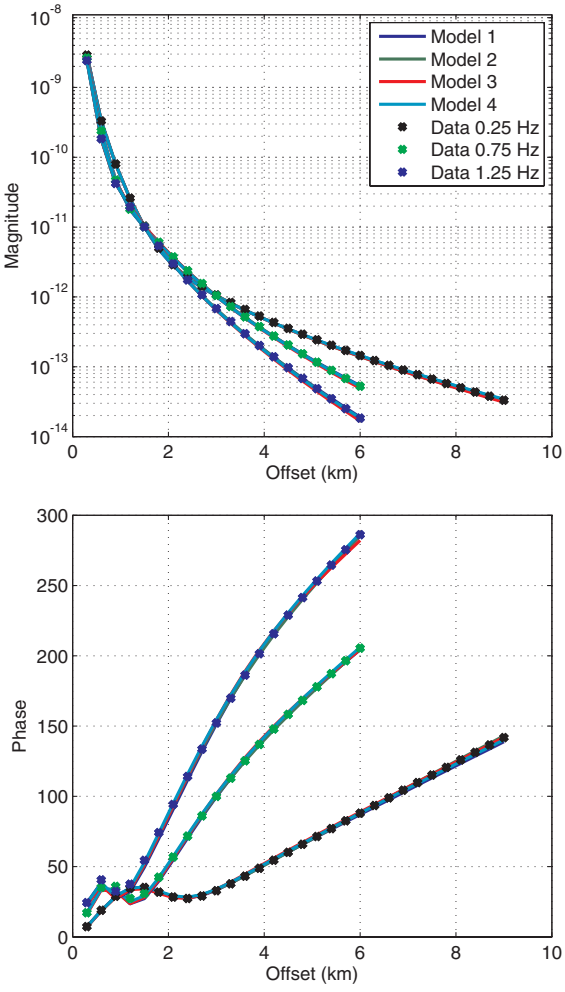

Figure 4. Data match. Comparison of observed data to the modeled response from the four resistivity profiles in Figure 3.

inline and broadside electric and magnetic components with the extended frequency set. The marginal distribution as a function of depth for run 16 is displayed in Figure 6. Compared to run 5, we see that the uncertainty in the inversion is reduced in the upper part of the profile, and that the inversion generally follows the original resistivity profile better. The target layer is also slightly better pronounced with mean vertical resistivity 24.7 Ωm, but still far below the results in runs 1–3 with narrow prior model for the nontarget layers.

To better illustrate the effect of including more data, we display the joint distribution of the vertical transverse-resistance T_v in the target layer and the layer directly below. The transverse-resistance is defined as the product of the resistivity and the thickness, $T_v = R_v \Delta t$. Figures 7 and 8 show this distribution for run 5 and run 16 on a logarithmic scale. The main effect of including the extended data set is that the probability that both layers have a transverse-resistance below 2000 Ωm^2 is effectively ruled out. For both data sets, the transverse-resistance in the target is slightly larger than the central peak in the distribution. The posterior distributions are also far from symmetric, thus a linearized approach to assess the uncertainty is of limited value.

When the resistivity is well bounded, as for the focused model used in runs 1–3, the inversion is well constrained by the electrical inline component and the standard frequency set. Addition of multiple components, extended frequency set, and MT data do not improve the inversion results substantially, i.e., compare runs 2 and 3.

The prior distribution for the nontarget layers influence the results significantly. When the wide prior distribution is used, the median in the target region is systematically lower than when the focused prior distribution is used. This is because the wide prior distribution allows the nontarget layers to have high resistivities and thus provides alternative explanations for the data that does not have a strong resistivity anomaly in the target layer.

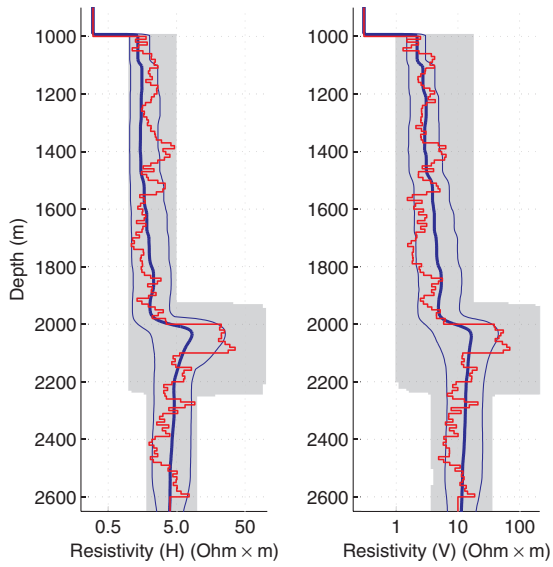

Figure 5. Inversion results for the wide prior, with the standard CSEM survey. On the left horizontal resistivity, and the vertical resistivity is on the right. The thick blue curve is the median at each point, the thin blue curves is P10 and P90. The original curve is red, and the gray shaded area shows the prior range.

The focused prior distribution gives systematically higher and better estimates of the target resistivity and a larger reduction in the uncertainty (nIQR). The focused prior model bounds the non-target layers to low resistivities and limits the solution space.

In general, the inclusion of MT data does not effect the results in the target substantially. For the wide prior model, inversion of the MT-data alone have no practical effects and reduces the uncertainty (nIQR) only to 99% of the prior uncertainty. The main effect of the MT data is that they constrain the horizontal resistivity in the lower half-space.

There is no clear conclusion with respect to whether the additional components give a better effect than the extended frequency set, but the inclusion of the extended frequency set appears to have a larger effect when we use several components than when only the inline electric components are used.

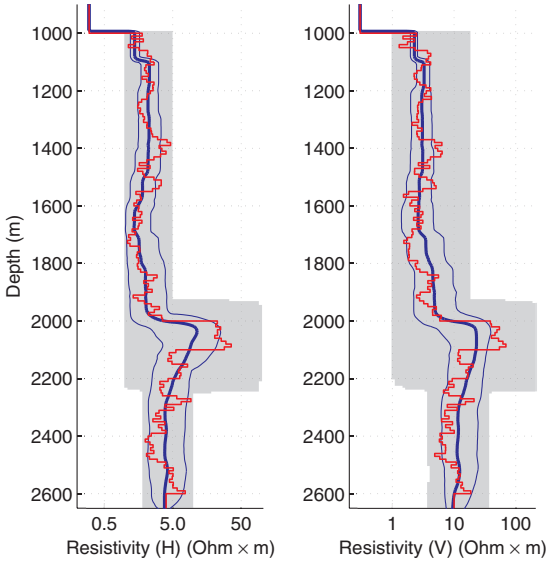

Figure 6. Inversion results for the wide prior, with MT and CSEM inline and broadside electric and magnetic data with extended frequency set. On the left horizontal resistivity, and the vertical resistivity is on the right. The thick black curve is the median at each point, the thin black curves is P10 and P90, and the original curve is in red. The shaded gray area is the prior range.

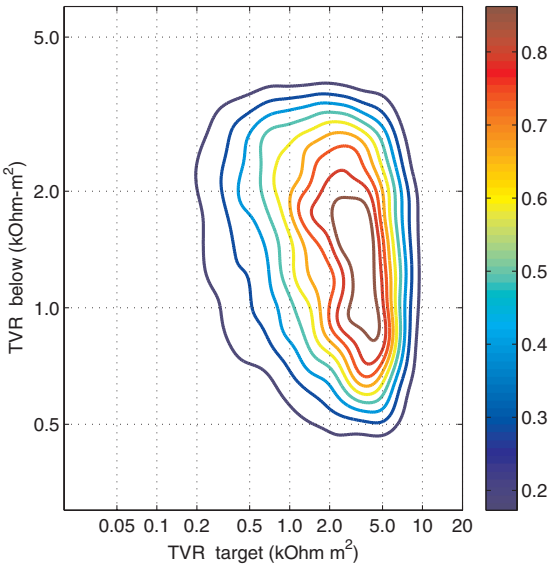

Figure 7. Posterior density estimate of the vertical transverse-resistance ($T_v = R_v\Delta t$) in target versus the layer below for run 5. The contours are plotted such that the inner contour contains 10% of the accepted models, next contour contains 20% and so on until the outer contour, which contains 90% of all accepted models.

CMP INVERSION OF TROLL DATA

A CSEM line over the Troll West Gas Province was acquired in 2008 by EMGS and Statoil in a joint research project. We use the frequencies 0.25, 0.75, 1.25, 1.75, and 2.25 Hz for the inline electric component. The data are represented with 500-m steps in the offset, from 500 to 9500 m. The error in the data consist of an relative error of 10%, and a noise floor at 10^{-15}. The error quantities are based on standard numbers.

The background resistivities in the Troll area are generally low, but there are also some shallow anomalies with moderate resistivity. The anisotropy in the region is also small. We use depth converted seismic horizons to outline the layer structure, and add uncertainty to the thicknesses of each layer. The prior limits are listed in Table 3. All distributions used are uniform on the specified interval.

The resistivity was solved for every kilometer and the result was interpolated in each layer between these marks to provide the results. The mean horizontal and vertical resistivities are plotted in Figures 9 and 10, which also display the depth-converted horizons. Because the local 1D approach does not account for lateral effects when modeling the EM response, high-resistivity regions appear to be wider than they actually are. An example of this is seen in the inversion in Figures 9 and 10, where the high resistivity region extends west of the fault at 6 km and eastward from 13 to 16 km.

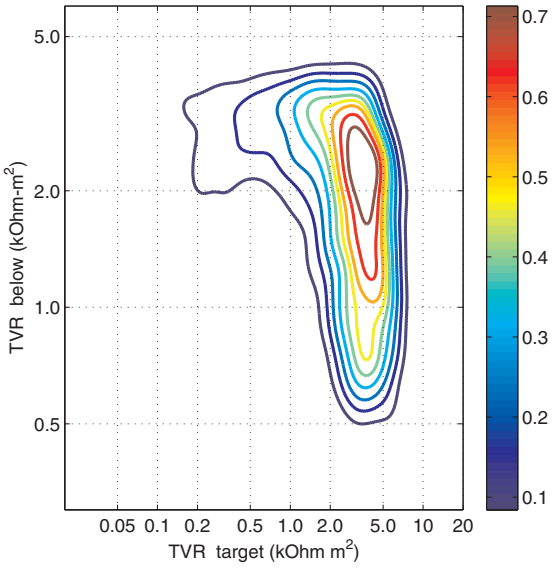

Figure 8. Posterior density estimate of vertical transverse-resistance ($T_v = R_v\Delta t$) in target versus the layer below for run 16. The contours are plotted such that the inner contour contains 10% of the accepted models, next contour contains 20% and so on until the outer contour, which contains 90% of all accepted models.

Table 3. Summary of prior model for Troll inversion. The table shows uncertainty for layer thickness, and value ranges for resistivity and anisotropy ratio. Number of layers are in parentheses.

Layer (no.)	Δt (m)	R_H (Ωm)	Ratio (1)
Air (1)	-	10^{13}	1
Water (1)	±10	0.25–0.35	1
Shallow (3)	±5	0.5–10	1–2
Above (7)	±10	0.5–2	1–2
Target (1)	±10	0.5–200	1–2
Below (1)	±10	0.5–2	1–2
Half-space (1)	-	0.5–2	1–2

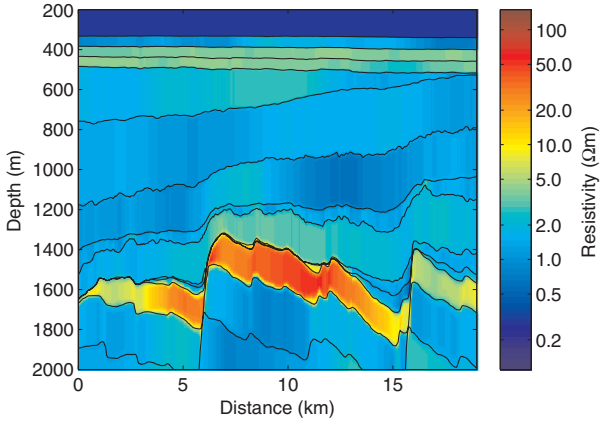

Figure 9. Posterior mean horizontal resistivity, and seismic horizons for the inverted line at Troll.

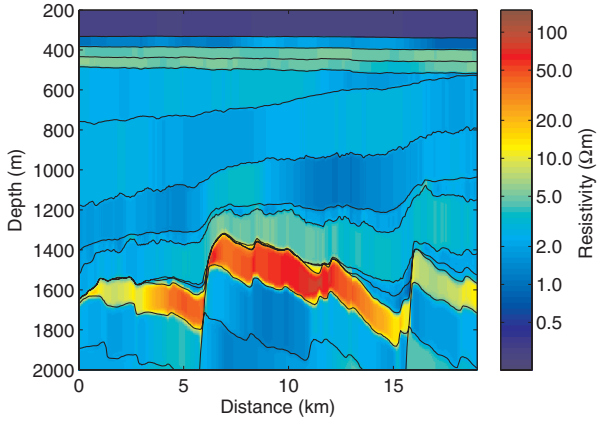

Figure 10. Posterior mean vertical resistivity, and seismic horizons for the inverted line at Troll.

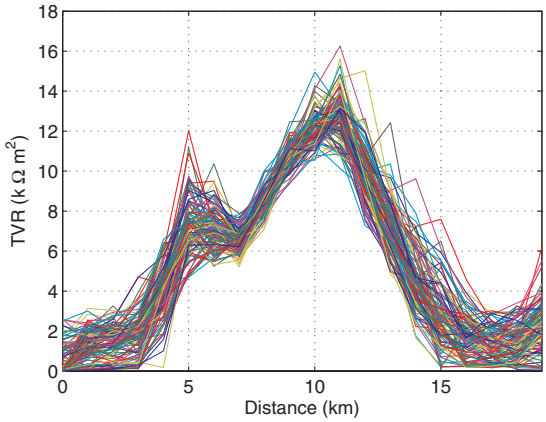

Figure 11. Posterior realizations of the transverse-resistance in the target layer.

The uncertainty in the target layer is illustrated in Figure 11, which displays 100 realizations of the transverse-resistance (resistivity-thickness product $T_v = R_v \Delta t$) in the target layer, and the uncertainty is well constrained along the full profile.

CONCLUSIONS

We have developed a Bayesian methodology for inversion of electromagnetic data based on a 1D forward modeling algorithm, and we have solved the inversion problem by a standard Markov chain Monte Carlo approach. We have demonstrated the approach by a synthetic inversion study and inversion of real data from Troll.

Inversion of EM data is a strongly nonlinear and ill-posed inverse problem. The Bayesian inversion algorithm finds a span of different resistivity models which all have a good fit to the data and within the uncertainty bounds of the data. This clearly illustrates the non-uniqueness problem and is a strong warning against most standard inversion methodologies providing only one solution without uncertainty bounds. The Bayesian inversion method provides the complete solution but is highly computer demanding even for 1D models.

The results show that there are severe nonlinearities in the problem. This indicates the danger of using a linearized approach to assess the uncertainty of the solution and it questions the validity of such approaches.

The study shows that the information defined in the prior distribution is essential. This includes both information about possible reservoir resistivities and possible background resistivities. Rock physics prior knowledge that can narrow the uncertainty bounds may be of crucial importance to get a successful and conclusive inversion result. The synthetic example shows that with a well-constrained prior distribution, it is possible to correctly detect the reservoir even with only the inline electric component and a limited set of frequencies.

The synthetic study shows that inclusion of more data generally improves the inversion results. However, for the focused prior distribution, the inclusion of broadside components, magnetic components, and extended set of frequencies gives only a marginal improvement. For the wide prior distribution, inclusion of the extended frequency set, inclusion of the broadside component, and the inclusion of the magnetic components all give a moderate improvement compared to inversion of standard frequency set of the

inline electric component only. There is no clear conclusion with respect to whether the additional components are more important than the extended frequency set, but the inclusion of the extended frequency set appears to have a larger effect when we use several components than when only the inline electric components are used. The inclusion of MT data does not show any significant effect related to the target resistivity. The main effect of the MT data is that it constrains the horizontal resistivity in the lower half-space.

ACKNOWLEDGMENTS

We thank Statoil for permission to publish this paper and the Statistics for Innovation center for financial support.

REFERENCES

Bosch, M., T. Mukerji, and E. F. Gonzalez, 2010, Seismic inversion for reservoir properties combining statistical rock physics and geostatistics: A review: Geophysics, **75**, no. 5, 75A165–75A176, doi: 10.1190/1.3478209.

Buland, A., and Y. El Ouair, 2006, Bayesian time-lapse inversion: Geophysics, **71**, no. 3, 43–48, doi: 10.1190/1.2196874.

Buland, A., O. Kolbjørnsen, R. Hauge, Ø. Skjæveland, and K. Duffaut, 2008, Bayesian lithology and fluid prediction from seismic prestack data: Geophysics, **73**, no. 3, C13–C21, doi: 10.1190/1.2842150.

Buland, A., O. Kolbjørnsen, and H. Omre, 2003, Rapid spatially coupled AVO inversion in the Fourier domain: Geophysics, **68**, 824–836, doi: 10.1190/1.1581035.

Buland, A., and H. Omre, 2003a, Bayesian linearized AVO inversion: Geophysics, **68**, 185–198, doi: 10.1190/1.1543206.

Buland, A., and H. Omre, 2003b, Bayesian wavelet estimation from seismic and well data: Geophysics, **68**, 2000–2009, doi: 10.1190/1.1635053.

Buland, A., and H. Omre, 2003c, Joint AVO inversion, wavelet estimation and noise-level estimation using a spatially coupled hierarchical bayesian model: Geophysical Prospecting, **51**, 531–550, doi: 10.1046/j.1365-2478.2003.00390.x.

Cagniard, L., 1953, Basic theory of the magnetotelluric method of geophysical prospecting: Geophysics, **18**, 605–635, doi: 10.1190/1.1437915.

Chave, A. D., and C. S. Cox, 1982, Controlled electromagnetic sources for measuring conductivity beneath the oceans. 1. Forward problem and model study: Journal of Geophysical Research, **87**, 5327–5338, doi: 10.1029/JB087iB07p05327.

Chen, J., G. M. Hoversten, D. Vasco, Y. Rubin, and Z. Hou, 2007, A Bayesian model for gas saturation estimation using marine seismic AVA and CSEM data: Geophysics, **72**, no. 2, WA85–WA95, doi: 10.1190/1.2435082.

Christensen, N. B., and K. Dodds, 2007, 1D inversion and resolution analysis of marine CSEM data: Geophysics, **72**, no. 2, WA27–WA38, doi: 10.1190/1.2437092.

Commer, M., and G.A. Newman, 2009, Three-dimensional controlled-source electromagnetic and magnetotelluric joint inversion: Geophysical Journal International, **178**, 1305–1316, doi: 10.1111/gji.2009.178.issue-3.

Constable, S., and C. J. Weiss, 2006, Mapping thin resistors and hydrocarbons with marine EM methods: Insights from 1D modeling: Geophysics, **71**, no. 2, G43–G51, doi: 10.1190/1.2187748.

Duijndam, A. J. W., 1988a, Bayesian estimation in seismic inversion. Part I: Principles: Geophysical Prospecting, **36**, 878–898, doi: 10.1111/gpr.1988.36.issue-8.

Duijndam, A. J. W., 1988b, Bayesian estimation in seismic inversion. Part II: Uncertainty analysis: Geophysical Prospecting, **36**, 899–918, doi: 10.1111/gpr.1988.36.issue-8.

Eidesmo, T., S. Ellingsrud, L. MacGregor, S. Constable, M. Sinha, S. Johansen, F. Kong, and H. Westerdahl, 2002, Seabed logging (SBL), a new method for remote and direct identification of hydrocarbon filled layers in deepwater areas using controlled source electromagnetic sounding: First Break, **20**, 144–152.

Ellingsrud, S., T. Eidesmo, M. Sinha, L. MacGregor, and S. Constable, 2002, Remote sensing of hydrocarbon layers by seabed logging (SBL): Results from a cruise offshore Angola: The Leading Edge, **21**, 972–982, doi: 10.1190/1.1518433.

Gilks, W. R., S. Richardson, and D. J. Spiegelhalter, 1996, Markov chain Monte Carlo in practice: Chapman & Hall.

Grana, D., and E. D. Rossa, 2010, Probabilistic petrophysical-properties estimation integrating statistical rock physics with seismic inversion: Geophysics, **75**, no. 3, O21–O37, doi: 10.1190/1.3386676.

Gunning, J., and M. E. Glinsky, 2004, Delivery: An open-source model-based Bayesian seismic inversion program: Computers & Geosciences, **30**, 619–636, doi: 10.1016/j.cageo.2003.10.013.

Gunning, J., and M. E. Glinsky, 2006, Wavelet extractor: A Bayesian well-tie and wavelet extraction program: Computers & Geosciences, **32**, 681–695, doi: 10.1016/j.cageo.2005.10.001.

Gunning, J., M. E. Glinsky, and J. Hedditch, 2010, Resolution and uncertainty in 1D CSEM inversion: A Bayesian approach and open-source implementation: Geophysics, **75**, no. 6, F151–F171, doi: 10.1190/1.3496902.

Hastings, W. K., 1970, Monte Carlo sampling methods using Markov chains and their applications: Biometrika, **57**, 97–109, doi: 10.1093/biomet/57.1.97.

Hou, Z., Y. Rubin, M. Hoversten, D. Vasco, and J. Chen, 2006, Reservoir parameter identification using minimum relative entropy-based Bayesian inversion of seismic AVA and marine CSEM data: Geophysics, **71**, no. 6, O77–O88, doi: 10.1190/1.2348770.

Hoversten, G., F. Cassassuce, E. Gasperikova, G. Newman, J. Chen, D. Vasco, Y. Rubin, and Z. Hou, 2006, Direct reservoir parameter estimation using joint inversion of marine seismic AVA and CSEM data: Geophysics, **71**, no. 3, C1–C13, doi: 10.1190/1.2194510.

Key, K., 2009, 1D inversion of multicomponent, multifrequency marine CSEM data: Methodology and synthetic studies for resolving thin resistive layers: Geophysics, **74**, no. 2, F9–F20, doi: 10.1190/1.3058434.

Key, K., S. Constable, and C. J. Weiss, 2006, Mapping 3D salt using the 2D marine magnetotelluric method: Case study from Gemini Prospect, Gulf of Mexico: Geophysics, **71**, no. 1, B17–B27, doi: 10.1190/1.2168007.

Kjønsberg, H., R. Hauge, O. Kolbjørnsen, and A. Buland, 2010, Bayesian Monte Carlo method for seismic predrill prospect assessement: Geophysics, **75**, no. 2, O9–O19, doi: 10.1190/1.3339678.

Larsen, A. L., M. Ulvmoen, H. Omre, and A. Buland, 2006, Bayesian lithology/fluid prediction and simulation on the basis of a Markov-chain prior model: Geophysics, **71**, no. 5, R69–R78, doi: 10.1190/1.2245469.

Løseth, L., and B. Ursin, 2007, Electromagnetic fields in planarly layered anisotropic media: Geophysical Journal International, **170**, 44–80, doi: 10.1111/gji.2007.170.issue-1.

Mackie, R., D. Watts, and W. Rodi, 2007, Joint 3D inversion of marine CSEM and MT data: 77th Annual International Meeting, SEG, Expanded Abstracts, 574–578, doi: 10.1190/1.2792486.

Malinverno, A., 2000, A Bayesian criterion for simplicity in inverse problem parametrization: Geophysical Journal International, **140**, 267–285, doi: 10.1046/j.1365-246x.2000.00008.x.

Metropolis, N., M. N. Rosenbluth, A. W. Rosenbluth, A. H. Teller, and E. Teller, 1953, Equation of state calculations by fast computing machines: Journal of Chemical Physics, **21**, 1087–1092, doi: 10.1063/1.1699114.

Mittet, R., H. Maulana, K. Brauti, and T. A. Wicklund, 2007, CMP inversion of marine CSEM data: 69th Annual Conference and Exhibition, EAGE, Extended Abstracts.

Rimstad, K., and H. Omre, 2010, Impact of rock-physics depth trends and Markov random fields on hierarchical Bayesian lithology/fluid prediction: Geophysics, **75**, no. 4, R93–R108, doi: 10.1190/1.3463475.

Robert, C. P., and G. Casella, 1999, Monte Carlo statistical methods: Springer-Verlag.

Scales, J. A., and L. Tenorio, 2001, Prior information and uncertainty in inverse problems: Geophysics, **66**, 389–397, doi: 10.1190/1.1444930.

Tarantola, A., 1987, Inverse problem theory: Elsevier Science Publishing Co. Inc.

Tarantola, A., and B. Valette, 1982, Inverse problems = quest for information: Journal of Geophysics, **50**, 159–170.

Ulrych, T. J., M. D. Sacchi, and A. Woodbury, 2001, A Bayes tour of inversion: A tutorial: Geophysics, **66**, 55–69, doi: 10.1190/1.1444923.

Veire, H., H. G. Borgos, and M. Landrø, 2006, Stochastic inversion of pressure and saturation changes from time-lapse AVO data: Geophysics, **71**, no. 5, C81–C92, doi: 10.1190/1.2235858.

Vozoff, K., 1972, The magnetotelluric method in the exploration of sedimentary basins: Geophysics, **37**, 98–141, doi: 10.1190/1.1440255.